A General and Parallel Platform for Mining Co-Movement Patterns over Large-scale Trajectories

ABSTRACT

1. INTRODUCTION

The prevalence of positioning devices has drastically boosted the scale and spectrum of trajectory collection to an unprecedented level. Tremendous amounts of trajectories, in the form of sequenced spatial-temporal records, are continually generated from animal telemetry chips, vehicle GPSs and wearable devices. Data analysis on large-scale trajectories benefits a wide range of applications and services, including traffic planning [1], animal analysis [2], and social recommendations [3], to name just a few.

A crucial task of data analysis on top of trajectories is to discover co-moving patterns. A *co-movement* pattern [4] refers to a group of objects traveling together for a certain period of time and the group is normally determined by spatial proximity. A pattern is prominent if the size of the group exceeds M and the length of the duration exceeds K, where M and K are parameters specified by users. Rooted from such basic definition and driven by different mining applications, there are a bunch of variants of co-movement patterns that have been developed with more advanced constraints.

Table 1 summarizes several popular co-moving pattern s with different constraints in the attributes of clustering in spatial proximity, consecutiveness in temporal duration and computational complexity. In particular, the *flock* [5] and the *group* [6] patterns require all the objects in a group to be enclosed by a disk with radius r; whereas the *convoy* [7], the *swarm* [8] and the *platoon* [9] patterns resort to density-based spatial clustering. In the temporal dimension, the *flock* [5] and the *convoy* [7] require all the timestamps of each detected spatial group to be consecutive, which is referred to as *global consecutiveness*; whereas the *swarm* [8] does not impose any restriction. The *group* [6] and the *platoon* [9] adopt a compromised manner by allowing arbitrary gaps between the consecutive segments, which is called *local consecutiveness*. They introduce a parameter L to control the minimum length of each local consecutive segment.

Patterns	Proximity	Consecutiveness	Time Complexity
flock [10]	disk-based	global	$O(\lvert\mathbb{O}\rvert\lvert\mathbb{T}\rvert(M + log(\lvert\mathbb{O}\rvert))$
convoy [7]	density-based	global	$O(\lvert\mathbb{O}\rvert^2 + \lvert\mathbb{O}\rvert\lvert\mathbb{T}\rvert)$
swarm [8]	density-based	-	$O(2^{\lvert\mathbb{O}\rvert}\lvert\mathbb{O}\rvert\lvert\mathbb{T}\rvert)$
group [6]	disk-based	local	$O(\lvert\mathbb{O}\rvert^2\lvert\mathbb{T}\rvert)$
platoon [9]	density-based	local	$O(2^{\lvert\mathbb{O}\rvert}\lvert\mathbb{O}\rvert\lvert\mathbb{T}\rvert)$

Table 1: Constraints and complexity of co-movement patterns. The time complexity indicates the performance in the worst case, where $|\mathbb{O}|$ is the total number of objects and $|\mathbb{T}|$ is the number of descritized timestamps.

Figure 1 is an example to demonstrate the concepts of various co-movement patterns. The trajectory database consists of six moving objects and the temporal dimension is discretized into six snapshots. In each snapshot, we treat the clustering methods as a black-box and assume that they generate the same clusters. Objects in proximity are grouped in the dotted circles. As aforementioned, there are three parameters to determine the co-movement patterns and the default settings in this example are $M = 2$, $K = 3$ and $L = 2$. Both the *flock* and the *convoy* require the spatial clusters to last for at least K consecutive timestamps. Hence,$\{o_3, o_4\}$ and $\{o_5, o_6\}$ remains the only two candidates matching the patterns. The *swarm* relaxes the pattern matching by discarding the temporal consecutiveness constraint. Thus, it generates many more candidates than the *flock* and the *convoy*. The *group* and the *platoon* add another constraint on local consecutiveness to retain meaningful patterns. For instance, $\{o_1, o_2 : 1, 2, 4, 5\}$ is a pattern matching local consecutiveness because timestamps $\{1, 2\}$ and $\{4, 5\}$ are two segments with length no smaller than $L = 2$. The difference between the *group* and the *platoon* is that the *platoon* has an additional parameter K to specify the minimum number of snapshots for the spatial clusters. This explains why $\{o_3, o_4, o_5 : 2, 3\}$ is a *group* pattern but not a *platoon* pattern.

As can be seen, there are various co-movement patterns requested by different applications and it is cumbersome to design a tailored solution for each type. In addition, despite the generality of the *platoon* (i.e., it can be reduced to other types of patterns via proper parameter settings), it suffers from the so-called *loose-connection* anomaly. We use two objects o_1 and o_2 in Figure 2 as an example to illustrate the scenario. These two objects form a *platoon* pattern in timestamps $\{1, 2, 3, 102, 103, 104\}$. However, the two consecutive segments are 98 timestamps apart, resulting in a false positive co-movement pattern. In reality, such an anomaly may be caused by the periodic movements of unrelated ob-

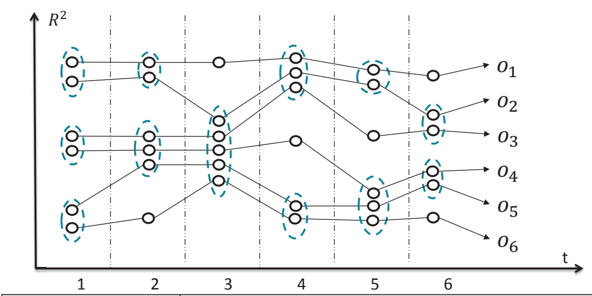

Flock(M=2, K=3)	$\{o_3, o_4$: 1,2,3$\}$ $\{o_5, o_6$: 3,4,5$\}$
Convoy(M=2, K=3)	$\{o_3, o_4$: 1,2,3$\}$ $\{o_5, o_6$: 3,4,5$\}$
Group(M=2, L=2)	$\{o_1, o_2$: 1,2,4,5$\}$ $\{o_3, o_4, o_5$: 2,3$\}$ $\{o_5, o_6$: 3,4,5$\}$
Platoon (M=2,K=3,L=2)	$\{o_1, o_2$: 1,2,4,5$\}$ $\{o_3, o_4$: 1,2,3$\}$ $\{o_4, o_5$: 2,3,5,6$\}$ $\{o_5, o_6$: 3,4,5$\}$
Swarm (M=2,K=3)	$\{o_1, o_2$: 1,2,4,5$\}$ $\{o_3, o_4$: 1,2,3$\}$ $\{o_4, o_5$: 2,3,5,6$\}$ $\{o_5, o_6$: 1,3,4,5$\}$ $\{o_2, o_3$: 3,4,6$\}$

Figure 1: Trajectories and co-movement patterns; The example consists of six trajectories across six snapshots. Objects in spatial clusters are enclosed by dotted circles. M is the minimum cluster cardinality; K denotes the minimum number of snapshots for the occurrence of a spatial cluster; and L denotes the minimum length for local consecutiveness.

jects, such as vehicles stopping at the same petrol station or animals pausing at the same water source. Unfortunately, none of the existing patterns have directly addressed this anomaly.

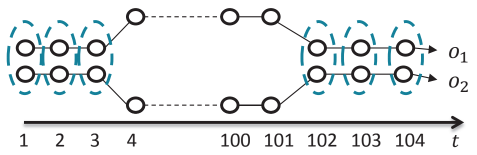

Figure 2: *Loose-connection* anomaly. Even though $\{o_1, o_2 : 1, 2, 3, 102, 103, 104\}$ is considered as a valid *platoon* pattern, it is highly probable that these two objects are not related as the two consecutive segments are 98 timestamps apart.

The other issue with existing methods is that they are built on top of centralized indexes which may not be scalable. Table 1 shows their theoretical complexities in the worst cases and the largest real dataset ever evaluated in previous studies is up to million-scale points collected from hundreds of moving objects. In practice, the dataset is of much higher scale and the scalability of existing methods is left unknown. Thus, we conduct an experimental evaluation with 4000 objects moving for 2500 timestamps to examine the scalability. Results in Figure 3 show that their performances degrade dramatically as the dataset scales up. For instance, the detection time of *group* drops twenty times as the number of objects grows from *1k* to *4k*. Similarly, the performance of *swarm* drops over fifteen times as the number of snapshots grows from *1k* to *2.5k*. These observations imply that existing methods are not scalable to support large-scale trajectory databases.

Therefore, our primary contributions in this paper are to close these two gaps. First, we propose the *general co-movement pattern* (GCMP) which models various co-moment patterns in a unified way and can avoid the *loose-connection*

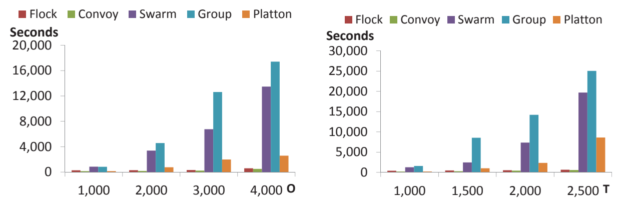

(a) $1k$ timestamps (b) $1k$ objects

Figure 3: Performance measures on existing co-movement patterns. A sampled Geolife data set is used with up two 2.4 million data points. Default parameters are $M = 10$ $K = 20$ $L = 10$.

anomaly. In GCMP, we introduce a new gap parameter G to pose a constraint on the temporal gap between two consecutive segments. By setting a feasible G, the loose-connection anomaly can be avoided. In addition, our GCMP is both general and expressive. It can be reduced to any of the previous patterns by customizing the parameters.

Second, we investigate deploying our GCMP detector on MapReduce platforms (such as Hadoop and Spark) to tackle the scalability issue. Our technical contributions are threefold. First, we replicate the snapshots in multiple data chunks to support efficient parallel processing. Second, we devise a novel *Star Partition and Mining* (SPM) algorithm as a fine-granularity partitioning strategy to achieve workload balance. For each star, an Apriori method is adopted to mine the co-movement patterns. Third, we leverage the *temporal monotonicity* property of GCMP to design several optimization techniques including *edge-simplification* to prune initial candidates, *temporal apriori pruning* and *forward closure checking* to reduce the number of enumerated candidates in the Apriori algorithm.

We conduct a set of extensive experiments on three large-scaled real datasets with hundreds of millions temporal points. The results show that our parallel scheme efficiently supports GCMP mining in large datasets. In particular, with near 200 million trajectory points, our scheme runs within 10 minutes using 135 cores. Whereas centralized solution takes near 7 hours for 1 million trajectory points. Moreover, our optimized SPM methods achieves upto XXX times efficiency as compared to the baseline algorithm with near linear scalability.

The rest of our paper is organized as follows: Section 2 summarizes the relevant literature on trajectory pattern mining. Section 3 states the problem definition of our general co-movement pattern mining. Section 4 provides a baseline solution. An advanced solution named *star partition and mining* is presented in Section 5. Section **??** discusses various optimization techniques. Section 6 conducts extensive experiments to verify the efficiency of our system. Finally Section 7 concludes the paper.

2. RELATED WORKS

The *co-movement patterns* in literature consist of five members, namely *group* [6], *flock* [10], *convoy* [7], *swarm* [8] and *platoon* [9]. We have demonstrated the semantics of these patterns in Table 1 and Figure 1. In this section, we focus on comparing the techniques used in these works. For more trajectory patterns other than *co-movement patterns*, interested readers may move to [11] for a comprehensive survey.

2.1 Flock and Convoy

The difference between *flock* and *convoy* lies in the object clustering methods. In *flock* objects are clustered based on their distance. Specifically, the objects in the same cluster needs to have a pair-wised distance less than *min_dist*. This essentially requires the objects to be within a disk-region of delimiter less than *min_dist*. In contrast, *convoy* cluster the objects using density-based clustering [12]. Technically, *flock* utilizes a m^{th}-order Voronoi diagram [13] to detect whether a subset of object with size greater than m stays in a disk-region. *Convoy* employs a trajectory simplification [14] technique to boost pairwise distance computations in the density-based clustering. After clustering, both *flock* and *convoy* use a line-sweep method to scan each snapshots. During the scan, the object group appears in consecutive timestamps is detected. Meanwhile, the object groups that do not match the consecutive constraint are pruned. However, such a method faces high complexity issues when supporting other patterns. For instance, in *swarm*, the candidate set during the line-sweep grows exponentially, and many candidates can only be pruned after the entire snapshots are scanned.

2.2 Group, Swarm and Platoon

Different from *flock* and *convoy*, all the *group*,*swarm* and *platoon* patterns have more constraints on the pattern duration. Therefore, their techniques of mining are of the same skeleton. The main idea of mining is to grow object set from an empty set in a depth-first manner. During the growth, various pruning techniques are provided to prune unnecessary branches. *Group* pattern uses the Apriori property among patterns to facilitate the pruning. *Swarm* adapts two more pruning rules called backward pruning and forward pruning. *Platoon* further adapts a prefix table structure to guide the depth-first search. As shown by Li et.al. [9], *platoon* outperforms other two methods in efficiency. However, the three patterns are not able to directly discover the general co-movement pattern. Furthermore, their pruning rules heavily rely on the depth-first search nature, which lost its efficiency in the parallel scenario.

2.3 MaReduce Framework

MapReduce (MR) was formally proposed by Dean et.al. [15] and has subsequently implemented by many open source systems. Those systems provide handy APIs with fault tolerances and are popularly used as large-scale data processing platforms. In simple words, there are two conceptual types of computing nodes in MR, namely the *mapper*s and the *reducer*s. The execution of a MR algorithm consists of three major steps: First, input data are partitioned and read by a *map* function on each mapper. Then, mappers emit key-value pairs which are *shuffle*d over the network to reducers. Lastly, reducers process the received data using a *reduce* function.

3. DEFINITIONS

Let $\mathbb{O} = \{o_1, o_2, ..., o_n\}$ be the set of objects and $\mathbb{T} = \{1, 2, ..., m\}$ be the descritized temporal dimension. A time sequence T is defined as a subset of $\mathbb{T}$, i.e., $T \subseteq \mathbb{T}$, and we use $|T|$ to denote sequence length. Let T_i be i-th entry in T and we say T is consecutive if $\forall 1 \leq i \leq |T|-1$, $T_{i+1} = T_i+1$. It is obvious that any time sequence T can be decomposed into consecutive segments and we say T is *L-consecutive* [9] if the length of all the consecutive segments is no smaller than L.

As illustrate in Figure 2, patterns adapting the notion of L-consecutiveness (e.g., *platoon* and *group*) still suffer from *loose connection* problem. To avoid such an anomaly without losing pattern generality, we introduce a parameter G to control the gaps between timestamps in a pattern. Formally, a G-connected time sequence is defined as follows:

Definition 1 (G-connected)**.** *A time sequence T is G-connected if the gap between any of its neighboring timestamps is no greater than G. That is $\forall T_i, T_{i+1} \in T, T_{i+1} - T_i \leq G$.*

We take $T = \{1, 2, 3, 5, 6\}$ as an example, which can be decomposed into two consecutive segments $\{1, 2, 3\}$ and $\{5, 6\}$. T is not 3-consecutive since the length $\{5, 6\}$ is 2. Thus, it is safe to say either T is 1-consecutive or 2-consecutive. On the other hand, T is 2-connected since the maximum gap between its neighboring time stamps is $5 - 3 = 2$. It is worth noting that T is not 1-connected because the gap between T_3 and T_4 is 2 (i.e., 5-3=2).

Given a trajectory database descritized into snapshots, we can conduct a clustering method, either disk-based or density-based, to identify groups with spatial proximity. Let T be the set of timestamps in which a group of objects O are clustered. We are ready to define a more general co-movement pattern:

Definition 2 (General Co-Movement Pattern)**.** *A general co-movement pattern finds a set of objects O satisfying the following five constraints: 1) closeness: the objects in O belong to the same cluster in the timestamps of T; 2) significance: $|O| \geq M$; 3) duration: $|T| \geq K$; 4) consecutiveness: T is L-consecutive; and 5) connection: T is G-connected.*

There are four parameters in our general co-movement pattern, including object constraint M and temporal constraints K, L, G. By customizing these parameters, our pattern can express other patterns proposed in previous literature, as illustrated in Table 2. In particular, by setting $G = |T|$, we achieve the *platoon* pattern. By setting $G = |T|, L = 1$, we achieve the *swarm* pattern. By setting $G = |T|$, $M = 2$, $K = 1$, we gain the *group* pattern. Finally by setting $G = 1$, we achieve the *convoy* and *flock* pattern. In addition to the flexibility of representing other existing patterns, our GCMP is able to avoid the *loose connection* anomaly by tuning the parameter G. It is notable that GCMP cannot be modeled by existing patterns.

It is also observable that the number of patterns in GCMP could be exponential under some parameter settings (i.e., when expressing *swarm*). In particular, given a parameter M, if a pattern P is valid, then any subset of P with size M is also a valid pattern. This results in additional $\Sigma_{M \geq i \geq |P.O|} \binom{|P.O|}{i}$ patterns, which is clearly overwhelming and redundant. For all these patterns, output P is sufficient. Therefore, we define the *Closed General Co-Movement Pattern* as follows:

Definition 3 (Closed General Co-Movement Pattern)**.** *A general co-moving pattern $P = \langle O : T \rangle$ is closed if and only if there does not exist another general co-moving pattern P' s.t. $P.O \subseteq P'.O$.*

Pattern	M	K	L	G	Clustering
Group	2	1	2	$\lvert\mathbb{T}\rvert$	Disk-based
Flock	$\cdot$	$\cdot$	K	1	Disk-based
Convoy	$\cdot$	$\cdot$	K	1	Density-based
Swarm	$\cdot$	$\cdot$	1	$\lvert\mathbb{T}\rvert$	Density-based
Platoon	$\cdot$	$\cdot$	$\cdot$	$\lvert\mathbb{T}\rvert$	Density-based

Table 2: Expressing other patterns using GCMP. $\cdot$ indicate a user specified value. M represents the object *size* constraints. K represents *duration* constraint. L represents *consecutiveness* constraint. G represents the *connection* constraints.

For example, let $M = 2, K = 2, , L = 1, G = 1$. In Figure 1, the pattern $P_1 = \{o_3, o_4 : 1, 2, 3\}$ is not a closed pattern. This is because $P_2 = \{o_3, o_4, o_5 : 2, 3\}$ is a closed pattern since $P_2.O \supset P_1.O$. The closed pattern avoids outputting duplicate information, thus making the result patterns more compact.

Our definition of GCMP is free from clustering method. Users are able to supply different clustering methods to facilitate different application needs. We currently expose both disk-region based clustering and DBSCAN as options to the user.

In summary, the goal of this paper is to present a parallel solution for discovering closed GCMP from large-scale trajectory data.

Before we move on to the algorithmic part, we list the notations that are used in the following sections.

Symbols	Meanings
S_t	snapshot of objects at time t
$\mathbb{O}$	set of objects
M	object size constraint
K	duration constraint
L	consecutiveness constraint
G	connection constraint
$P = (O : T)$	pattern with object set O, time sequence T
η	replication factor in TRM
$C_t(o)$	the cluster of object o at time t
S_t	the set of clusters at time t
λ_i	the partition with snapshots $S_t, .., S_{t+\eta-1}$
Sr_i	the star of object i

Table 3: Symbols and notions that will be used

4. BASELINE: TEMPORAL REPLICATION AND PARALLEL MINING

In this section, we propose a baseline solution that resorts to MapReduce (MR) as a general, parallel and scalable paradigm for GCMP pattern mining. The framework, named *temporal replication and parallel mining* (TRPM), is illustrated in Figure 4. There are two cycles of map-reduce jobs connected in a pipeline manner. The first cycle deals with spatial clustering in each snapshot, which can be seen as a preprocessing step for the subsequent pattern mining. In particular, the timestamp is treated as the key in the map phrase and objects within the same snapshot are clustered (DBSCAN or disk-based clustering) in the reduce phrase. Finally, the reducers output clusters of objects in each snapshot, represented by a list of S_t, where t is the timestamp and S_t is a set of clustered objects at snapshot t.

Our focus in this paper is the second map-reduce cycle of parallel mining, which essentially consists of two key questions to solve. The first is how to employ effective data partitioning such that the mining can be conducted independently; and the second is how to efficiently mine the valid patterns within each partition.

It is obvious that we cannot simply split the trajectory database into disjoint partitions because a GCMP pattern requires L-consecutive and the corresponding segments may cross multiple partitions. Our strategy is to use data replication to enable parallel mining. Each snapshot will replicate its clusters to η preceding snapshots. In other words, the partition for the snapshot S_t contains clusters in S_t, $S_{t+1} \ldots, S_{t+\eta}$. Determining a proper η is critical in ensuring the correctness and efficiency of TRPM. If η is too small, certain cross-partition patterns may be missed. If η is set too large, expensive network communication and CPU processing costs would be incurred in the map and reduce phrases respectively.

To guarantee that no valid pattern is missing, we enforce the following statement on η: I HAVE NO IDEA WHAT YOU ARE TALKING ABOUT STARTING FROM HERE!!! *Let T' be the* shortest *valid subsequence (wrt. K, L, G) of a valid temporal sequence T. Then, η needs to be the upper bound for all T' among all valid temporal sequences to ensure the completeness.* Finding the *minimum* η is not straightforward. We notice the minimum η is related to the temporal parameters K, L, G by making the following observation on $G = 1$:

Let T be an arbitrary valid temporal sequence. Since G equals to 1, T can be represented as $T = (t_1, t_2, ..., t_m)$, where $t_i + 1 = t_{i+1}$ and $m \geq K$. Let $T' = (t_1, ..., t_k)$, T' is the shortest valid temporal sequence of T. Note that T' is fully contained in the partition $\lambda_{t_1} = \{S_{t_1}, ..., S_{t_k}\}$, therefore it can be mined in λ_{t_1}. Since T is an arbitrary valid temporal sequence, the minimum η is thus K.

Inspired by the observation, we generalize the relationship between the minimum η and temporal parameters using the following theorem:

Theorem 1. *The minimum η to ensure the completeness of the temporal replication is:*

$$\eta = \begin{cases} (\lceil \frac{K}{L} \rceil - 1) * (G - 1) + 2K - 2, & \textit{if } G \geq 2 \\ K, & \textit{if } G = 1 \end{cases}$$

, where K, L, G are the temporal parameters.

Proof. When $G = 1$, we have demonstrated $\eta = K$ in the above observation. When $G \geq 2$, we compute η as follows: any T' can be viewed as n consecutive segments with sizes $l_1, .., l_n$ and $n-1$ gaps with sizes $g_1, ..., g_{n-1}$. Since η is the upper bond among all T's, η can be formulated as follows:

$$\eta = \max_{n, l_i, g_i} \{\Sigma_{i=1}^{i=n} l_i + \Sigma_{i=1}^{i=n-1} g_i\} \qquad (1)$$

With the following constraints: (1)$\forall l_i, L \leq l_i \leq K - 1$; (2) $\forall g_i, 1 \leq g_i \leq G - 1$; (3) $\Sigma_{i=1}^{i=n} l_i \geq K$ and (4) $\Sigma_{i=1}^{i=n-1} l_i \leq K - 1$. Constraints (1)(2)(3) due to the validity of T' and $G \geq 2$ (4) is because $|T'|$ is minimum. Based on (1)(3)(4), we can derive (5): $n \in [1, \lceil \frac{K}{L} \rceil]$. Constraints (1)-(5) form a convex polygon and η is monotone increasing wrt. n, l_i, g_i,

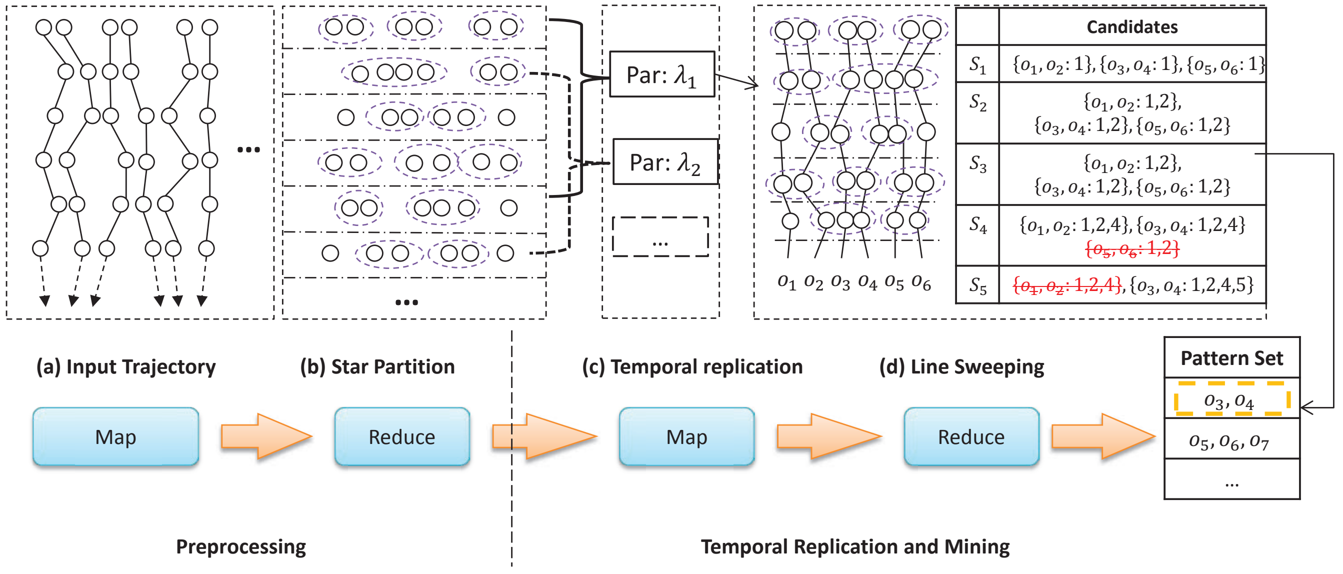

	Candidates
S_1	$\{o_1, o_2: 1\}, \{o_3, o_4: 1\}, \{o_5, o_6: 1\}$
S_2	$\{o_1, o_2: 1{,}2\}$, $\{o_3, o_4: 1{,}2\}, \{o_5, o_6: 1{,}2\}$
S_3	$\{o_1, o_2: 1{,}2\}$, $\{o_3, o_4: 1{,}2\}, \{o_5, o_6: 1{,}2\}$
S_4	$\{o_1, o_2: 1{,}2{,}4\}, \{o_3, o_4: 1{,}2{,}4\}$ ~~$\{o_5, o_6: 1{,}2\}$~~
S_5	~~$\{o_1, o_2: 1{,}2{,}4\}$~~, $\{o_3, o_4: 1{,}2{,}4{,}5\}$

Figure 4: Work flow of Temporal Replication and Mining. (a)(b) correspond to the first map-reduce cycle which clusters objects in each snapshot; (c)(d) correspond to the second map-reduce cycle which uses temporal replication to mine GCMP in parallel.

therefore, the maximum value of η is taken at the upper boundaries where $g_i = G-1$, $\Sigma_{i=1}^{i=n-1} l_i = K-1$, $l_i = K-1$ and $n = \lceil \frac{K}{L} \rceil$. This leads to $\eta = (\lceil \frac{K}{L} \rceil - 1) * (G-1) + 2K - 2$. $\square$

Based on the above theorem, during TRPM, every consecutive η snapshots form a partition. In particular, for every snapshot S_t, there is a partition $\lambda_t = \{S_t, ..., S_{t+\eta-1}\}$. With this partition strategy, when discovering GCMPS in λ_t, we only need to keep the pattern candidates whose object set are in S_t. This motivates to design an efficient *line-sweep* mining (LSM) method for each partition. The intuition of LSM is to sequentially scan all snapshots. During scanning, a set of pattern candidates is maintained. When all snapshots are scanned, the remaining candidates are the true patterns. The detail of LSM is presented in Algorithm 1. A candidate set C is maintained throughout the algorithm(line 1). C is initialized by inserting clusters at S_t (lines 2-4). During scanning snapshot S_j, candidates in C are joined with clusters at S_j. In the join, a candidate grows its temporal sequence while potentially reduces its object set. After the join, false patterns are deleted (line 7). Note that the size of C is always decreasing, therefore the complexity of LSM λ_t is $O(\eta|S_t||\overline{S}|)$,where $|\overline{S}|$ is the average snapshot size in λ_t.

The complete picture of temporal replication and parallel mining is summarized in Algorithm 2. We illustrate the workflow of TRPM method using Figure 4 (c)(d) with pattern parameters $M=2, K=3, L=2, G=2$. By Theorem 1, η is calculated as $(\lceil \frac{K}{L} \rceil - 1) * (G-1) + 2K - 2 = 5$. Therefore, in Figure 4 (c), every 5 consecutive snapshots are combined into a partition in the map phase. In Figure 4 (d), a line sweep method is illustrated for partition λ_1. Let C_i be the candidate set during sweeping snapshot S_i. Initially, C_1 contains patterns whose object set is in snapshot S_1. As line sweeps, the patterns in C_i grows. At snapshot S_4, the candidate $\{o_5, o_6\}$ is removed. This is because the gap between

Algorithm 1 Line Sweep Mining

```
Require: $\lambda_t = \{S_t, ..., S_{t+\eta-1}\}$
1: $C \leftarrow \{\}$                         ▷ Candidate set
2: for $c \in S_t$ do
3:     $C$.add($\langle c, t \rangle$)
4: end for
5: for all $j \in [t+1, t+\eta-1]$ do
6:     $C \leftarrow S_j \oplus C$
7:     remove false candidates from $C$
8: end for
9: output true candidates in $C$
```

its latest timestamp (i.e., 2) and the next scanning timestamp (i.e., 5) is 3, which violates the G constraint. Next, at snapshot S_5, the candidate $\{o_1, o_2\}$ is removed. This is because its local consecutive timestamps $\{4\}$ has only size 1, which violates the L constraint. Finally, $\{o_3, o_4\}$ is the qualified pattern and is outputted. Note that the minimum η under this setting is 5. If η is chosen as 4, the pattern $\{o_3, o_4\}$ would be excluded.

5. SPARE: STAR PARTITIONING AND APRIORI ENUMERATOR

The aforementioned replicate partitioning is based on the temporal dimension and results in groups of snapshots in each partition. To resolve the limitations caused by the replicate partitioning, we propose a new Star Partitioning and ApRiori Enumerator, named SPARE, to replace the second cycle of map-reduce jobs in Figure 4. Our new parallel mining framework is shown in Figure 5. Its input is the set of clusters generated in each snapshot and the output are mined GCMP patterns. In the following, we explain the two major components: star partitioning and apriori enumerator.

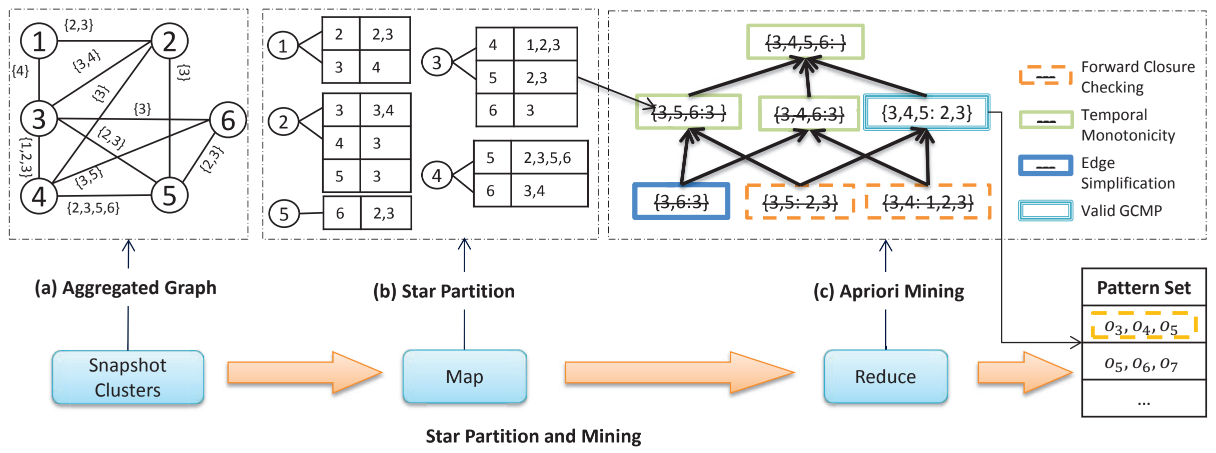

Figure 5: Star partition and mining. (a) Conceptual connection graph from Figure 1.(b) Five star partitions are generated (c) Apriori Mining with various pruning techniques.

Algorithm 2 Temporal Replication and Parallel Mining

```
Require: list of $\langle t, S_t \rangle$ pairs
 1: $\eta \leftarrow (\lceil \frac{K}{L} \rceil - 1) * (G - 1) + 2K - 2$
 2: —Map Phase—
 3: for all $\langle t, S_t \rangle$ do
 4:     for all $i \in 1...\eta - 1$ do
 5:         emit a $\langle \max(t - i, 0), S_t \rangle$ pair
 6:     end for
 7: end for
 8: —Partition and Shuffle Phase—
 9: for all $\langle t, S \rangle$ pair do
10:     group-by $t$, emit a $\langle t, \lambda_t \rangle$
11:     where $\lambda_t = \{S_t, S_{t+1}, ..S_{t+\eta-1}\}$
12: end for
13: —Reduce Phase—
14: for all $\langle t, \lambda_t \rangle$ do
15:     lineSweepMining($\lambda_t$)
16: end for
```

5.1 Star Partitioning

Let G_t be a graph for snapshot S_t, in which each node is a moving object and two objects are connected if they appear in the same cluster. It is obvious that G_t consists of a set of small cliques. Based on G_t, we define an aggregated graph G_A to summarize the cluster relationship among all the snapshots. In G_A, two objects form an edge if they are connected in any G_ts. Furthermore, we attach an inverted list for each edge, storing the associated timestamps in which the two objects are connected. An example of G_A, built on the trajectory database in Figure 1, is shown in Figure 5 (a). As long as two objects are clustered in any timestamp, they are connected in G_A. The object pair (o_1, o_2) appears in two clusters at timestamps 2 and 3 and is thus associated with an inverted list $\{2, 3\}$.

We use *star* as the data structure to capture the pair relationships. To avoid duplication, as G_t is an undirected graph and an edge may appear in multiple stars, we enforce a global ordering among the objects and propose a concept named *directed star*.

Definition 4 (Directed Star)**.** *Given a vertex with global id s, its directed star Sr_s is defined as the set of neighboring vertices with global id $t > s$. s is also called star id.*

Given an aggregated graph G_A, we can enumerate all the possible stars, as shown in Figure 5 (b). These stars are emitted from mappers to different reducers. The key is the star ID and the value is the neighbors in the star as well as the associated inverted lists. The reducer will then call the Apriori-based algorithm to enumerate all the valid GCMP patterns.

Before we introduce the Apriori enumerator, we are interested to examine the issue of global ordering on the moving objects. This is because assigning different IDs to the objects will result in different star partitioning results, which will eventually affect the workload balance among the map-reduce jobs. Specifically, we intended to measure the size of the *stragglers* [16, 17, 18] in star partition. Intuitively, the *stragglers* are the partitions that takes the most time to execute. We use Γ to indicate the number of edges of the *straggler* in star partition. And smaller Γ is always preferred. For example, Figure 6 gives two star partitioning results under different vertex ordering on the same graph. The top one has the $\Gamma = 5$ while the bottom one has the $\Gamma = 3$. It is obvious that the bottom one is much more balanced in terms of the size of each partition.

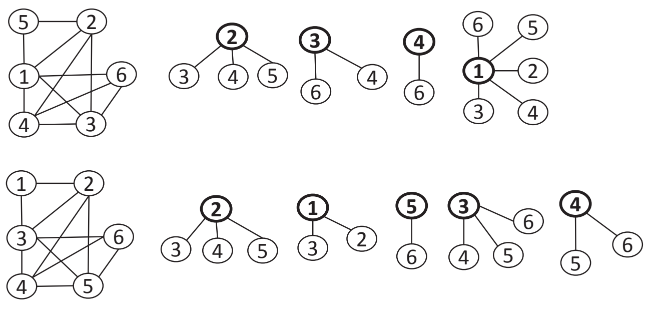

Figure 6: Examples of star partitioning with different vertex ordering.

To determine the optimal vertex orders with the objective of minimizing Γ, we can use a linear algebra model as follows: Let G_A be an aggregate graph, with a $n \times n$ adjacent matrix J. A vertex order is in fact a permutation of

J. Therefore, the adjacent matrices of any reordered graphs can be represented as PJP^T where $P \in \mathbb{P}$ is a *permutation matrix* [1] with dimension n. Since in star partition, we assign each edge $e(i,j)$ in G_A to the lower vertex, then the matrix $B = \text{triu}(PJP^T)$ [2] represents the assignment matrix wrt. P (i.e., $b_{i,j} = 1$ if vertex j is in star Sr_i). Let vector $\vec{b}$ be the *one*[3] vector of size n. Let $\vec{c} = B\vec{b}$, then each c_i denotes the number of edges in star Sr_i. Thus, Γ can be represented as the infinity norm of $B\vec{b}$. Let Γ^* be the minimum Γ among all vertex orders. Γ^* can then be formulated as follows:

$$\Gamma^* = \min_{P \in \mathbb{P}} ||B\vec{b}||_\infty \text{ ,where } ||B\vec{b}||_\infty = \max_{1 \le j \le n} (c_j) \qquad (2)$$

It is challenging to directly optimize the above equation. First, suppose there are $n!$ permutation matrices. Such a high complexity is trivially unpractical. Second, since G is unknown in prior, the vertex order cannot be planned beforehand. Despite these challenges, we find a simple $O(1)$ time solution which is good enough as stated in the following theorem.

Theorem 2 (Balance of Star Partition)**.** *Let G be an aggregated graph with n vertexes and the average degree d. Let Γ^* be optimal size of straggler among all vertex orders. Let Γ be the size of straggler wrt an random vertex order P. With high probability, the difference between Γ and Γ^* is $O(\sqrt{n \log n})$. That is, with probability $1 - 1/n$, $\Gamma = \Gamma^* + O(\sqrt{n \log n})$.*

In fact, we have a tighter bound of $(\Gamma - \Gamma^*)$ if the aggregate graph is *dense*. Specifically, if $d \ge \sqrt{12 \log n}$, with high probability, $\Gamma = \Gamma^* + O(\sqrt{d} \log n)$. Utilizing Theorem , in star partition, it is safe to choose the object IDs as the vertex order. This because real object IDs are often hashed and can be deemed as random.

5.2 Apriori Enumerator

Intuitively, given a GCMP pattern with an object set $\{o_1, o_2, \ldots, o_m\}$, all the pairs of (o_i, o_j) with $1 \le i < j \le m$ must be connected in the associated temporal graphs $\{G_t\}$. This inspires us to leverage the classic Apriori algorithm to enumerate all the valid GCMP patterns starting from pairs of objects. However, we observe that the monotonicity property does not hold between an object set and its supersets.

Example 1. *In this example, we show that if an object set is not a valid pattern, we cannot prune all its super sets. Consider two candidates $P_1 = \{o_1, o_2 : 1, 2, 3, 6\}$ and $P_2 = \{o_1, o_3 : 1, 2, 3, 7\}$. Let $L = 2, K = 3, G = 2$, then both candidates are not valid patterns. However, the timestamps of their super set $\{o_1, o_2, o_3\}$ is $P_1.T \cap P_2.T = \{1, 2, 3\}$, which conform to L, K, G. This indicates that even though $P_1.O$ and $P_2.O$ are not valid patterns, they cannot be pruned. Otherwise, $\{o_1, o_2, o_3\}$ would be missed out.*

5.2.1 Monotonicity

To ensure monotonicity, we first introduce a procedure named *star simplification*, to reduce the number of edges as well as unnecessary timestamps in the inverted lists. For instance, if the size of the inverted list for an edge e is smaller than K, then the edge can be safely removed because the number of timestamps in which its supersets are clustered must also be smaller than K. To generalize the idea, we propose two concepts named *maximal G-connected subsequence* and *candidate sequence*.

Definition 5 (Maximal G-connected Subsequence)**.** *A sequence T' is said to be a maximal G-connected subsequence of T if (1) T' is the subsequence of T, i.e., $\exists i \le j, T' = T(i, \ldots, j)$, (2) T' is G-connected, and (3) there exists no other subsequence T'' of T such that T' is the subsequence of T'' and T'' is G-connected.*

Example 2. *Let $G = 2$, consider $T_1 = (1, 2, 4, 5, 6, 9, 10, 11, 13)$. T has two maximal 2-connected subsequences: $T_1^A = \{1, 2, 4, 5, 6\}$ and $T_1^B = \{9, 10, 11, 13\}$. Consider $T_2 = (1, 2, 4, 5, 6, 8, 9)$, it can be verified that it is 2-connected, thus T_2 has only one maximal 2-connected subsequence which is itself.*

Definition 6 (Candidate Sequence)**.** *T is a candidate sequence if for any of its maximal G-connected subsequence T', we have (1) T' is L-consecutive; and (2) $|T'| \ge K$.*

Example 3. *Let $L = 2, K = 4$ and we follow the above example. T_1 is not a candidate sequence since one of its maximal 2-connected subsequence (i.e., T_1^B) is not 2-consecutive. In contrast, T_2 is a candidate sequence because it has one maximal 2-connected subsequence and it is L-connected with size greater than 2.*

Definition 7 (Sequence Simplification)**.** *Given a sequence T and the GCMP parameters G, L, K, a $T^{\#}$ is the simplified sequence of T if (1) $T^{\#}$ is contained in T, i.e., $T\# \subseteq T$. (2) $T^{\#}$ is a candidate sequence, and (3) no other candidate sequence $T_1^{\#}$ is contained in T and contains $T^{\#}$.*

Note that, not every T has the simplified sequence. For example, if $L = 3$, then the simplified sequence of $(1, 2, 5, 6)$ does not exists. Nevertheless, if there exists a $T^{\#}$ of T, then $T^{\#}$ is unique as stated in the following theorem:

Theorem 3. *For any sequence T, if T's simplified sequence is not empty, then there exists a unique $T^{\#}$ wrt T.*

Proof. We prove by contradiction. Suppose there are two simplified sequences $T_A^{\#}$ and $T_B^{\#}$ of the same T. We prove that, unless $T_B^{\#} \equiv T_A^{\#}$, $T_A^{\#}$ can always be enlarged, which leads to a contradiction. For simplicity, we use $\overline{ab}$ to denote the segment of a sequence from timestamp a to timestamp b. Consider the timestamps $T_C = T_B^{\#} - T_A^{\#}$. If $T_C = \emptyset$, then $T_A^{\#} \equiv T_B^{\#}$ naturally. Next, consider an arbitrary consecutive segment $\overline{ef}$ in T_C. Without loss of generality, we assume the next G-connected segment of $\overline{ef}$ in $T_B^{\#}$ is $\overline{cd}$ and the previous G-connected segment is $\overline{gh}$. There are four cases to be considered. We demonstrate the cases in Figure 7:

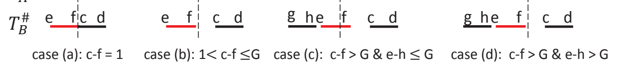

Figure 7: Proof of theorem 3.

- Case (a): $c - f = 1$, that is $\overline{ef}$ is part of a longer consecutive segment $\overline{ed}$. Since timestamp c is in $T_A^{\#}$, $T_A^{\#}$ can be safely enlarged by adding $\overline{ef}$.

[1]an identity matrix with rows shuffled
[2]triu is the upper triangle part of a matrix
[3]every element in $\vec{b}$ is 1

- Case (b): $G \geq c-f > 1$. In this case, since $c \geq a$, then $a-f \leq G$. Since the size of $\overline{ef}$ is greater or equal to L, adding $\overline{ef}$ to $\overline{ab}$ would still result in a valid candidate sequence.
- Case (c): $c - f > G$ and $e - h \leq G$. In this case, $\overline{ef}$ belongs to a G-connected sequence $\overline{gf}$ in $T_B^{\#}$. Observe that $\overline{gh}$ has no intersection with $T_A^{\#}$ (otherwise, it backs to case (a)), adding $\overline{gf}$ to $T_A^{\#}$ is equivalent in adding another candidate sequence to $T_A^{\#}$, making $T_A^{\#}$ still a valid simplified sequence.
- Case (d): $c - f > G$ and $e - h > G$. In this case, since $\overline{ef}$ is part of $T_B^{\#}$ and there is no segments G-connected with $\overline{ef}$, $\overline{ef}$ itself must be a candidate sequence. Therefore adding $\overline{ef}$ to $T_A^{\#}$ would still enlarge $T_A^{\#}$.

□

Next, we design an efficient simplification process with linear complexity. It takes two rounds scan of T as shown in Algorithm 3. In the first round, the consecutive portions of T with size less than L are removed. In the second round, the maximal G-connected sequences of size less than K are removed.

Algorithm 3 Edge Simplification

```
Require: $T$
 1: —$L$ Phase—
 2: $c \leftarrow 0$
 3: for $i \in (0, ..., |T|)$ do
 4:     if $T[i] - T[i-1] > 1$ then
 5:         if $i - c < L$ then
 6:             $T$ remove $[c : i)$
 7:         end if
 8:         $c \leftarrow i$
 9:     end if
10: end for
11: —$G$-$K$ Phase—
12: $s \leftarrow 1$, $c \leftarrow 0$
13: for $i \in (0 : |T|)$ do
14:     if $T[i] - T[i-1] > G$ then
15:         if $s < K$ then
16:             $T$ remove $[c : i)$
17:         end if
18:         $c \leftarrow i$, $s \leftarrow 1$
19:     else
20:         $s++$
21:     end if
22: end for
```

Example 4. *Take $T_1 = \{1, 2, 4, 5, 6, 9, 10, 11, 13\}$ as an example of edge simplification. Let $L = 2, K = 4, G = 2$. In the first round of scan. T_1 reduces to $\{1, 2, 4, 5, 6, 9, 10, 11\}$. The consecutive subsequence $\{13\}$ is removed by $L = 2$. T_1 has two maximal 2-consecutive subsequences, which are $\{1, 2, 4, 5, 6\}$ and $\{9, 10, 11\}$. Since $K = 4$, $\{9, 10, 11\}$ is removed from T_1 in the second round of scan. Therefore, T_1 is simplified to $\{1, 2, 4, 5, 6\}$, which is shortened 44%.*

With the concepts of *candidate sequence* and *sequence simplification*, we are ready to define the monotonic property that can be used for pruning.

Theorem 4. *Given a candidate pattern $P = \{O : T\}$, if sequence $P.T$ cannot be simplified to a candidate sequence, then any pattern candidate P' with $P.O \subseteq P'.O$ can be pruned.*

Proof. Let P_2 be a true pattern with $P_2.O \supseteq P.O$. It is easy to see that $P_2.T \subseteq P.T$. Since $P_2.T$ conforms to G, L, K. This indicates that $P_2.T$ is indeed a candidate sequence. Since $P_2.T \subseteq P.T$, $P.T$ can be simplified to candidate sequence (i.e., to $P_2.T$) which contradict with the fact that P cannot be simplified. Thus no such true pattern exists. □

5.2.2 *Apriori Algorithm*

To systematically discover valid patterns in each star, we design the *Apriori Mining* algorithm. To describe the algorithm, we call a candidate pattern R-pattern if the size of its object set is R. Therefore, each edge in the star is effectively a 2-pattern. The intuition of Apriori mining is the observation that $(R+1)$-patterns can be generated from R-patterns and 2 patterns. Thus, we may iteratively enumerate pattern candidates with all possible sizes. In particular, initially, for each $e(s, v) = ET$, pattern $p = (\{s, v\}, ET)$ is formed. During each iteration, we generate $(R + 1)$-patterns by joining R-patterns with the 2-patterns. Technically, the join between $p_1 = (O_1 : T_1)$ and $p_2 = (O_2 : T_2)$ generates a new pattern $p_3 = (O_1 \cup O_2 : T_1 \cap T_2)$. Note that in Sr_s, each R-pattern contains the object s, thus the join only grow a R-pattern at most to a $(R + 1)$-pattern. Our mining algorithm stops where no further patterns are generated. The algorithm is illustrated as in Algorithm 4.

Algorithm 4 Apriori Mining

```
Require: $Sr_s$
 1: Lv ← {},Ground ← {}, Output ← {}
 2: for all $e(s, t) = T \in Sr_s$ do
 3:     Simply $e(s, t)$                          ▷ Simplification
 4:     Ground.add($\langle\{s, t\}, T\rangle$)
 5:     Lv ← Ground
 6: end for
 7: while Lv is not empty do
 8:     Lv ← Lv $\oplus$ Ground                   ▷ Simplification
 9:     Remove false patterns in Lv               ▷ Monotonicity
10:     if union of Lv is a valid pattern then
11:         output.add(Lv)                        ▷ Forward Closure
12:         break
13:     end if
14: end while
15: output.addAll($Lv$)
16: return output
```

An illustration of Algorithm 4 is shown in Figure 5 (c). As shown, the star $Sr_3 = \{3, 4, 5, 6\}$ initially generate three 2-candidates. At every iteration, higher level candidates are generated by joining lower level candidates. When no more candidates can be generated, the algorithm stops by outputting the valid patterns.

EXPLAIN CLEARLY HOW YOU IMPLEMENT THE FORWARD CLOSURE CHECKING! BETTER SHOW IT IN THE ABOVE PSEDUDO CODE IN THE APRIORI ALGORITHM.

Although leveraging *temporal monotonicity* could largely prune false candidates and reduce the apriori search space, it is ineffective when a *true* pattern exists. In an extreme case, if a final pattern of a star Sr_s is the *union of all vertices* in the star, then in apriori, $\binom{|Sr_s|}{i+1}$ candidates needs to be generated at each level i. This results in an exponential search space while the output only contains one pattern. Generally, when candidates at level i collectively forms a true pattern, running aprior produces many wasted candidates.

Let Lv_i be the set of candidates at level i of Algorithm 4, we use the *forward closure* FC_i to denote the union of the objects in all candidates in Lv_i. Then, the *forward closure checking* is stated as follows:

Theorem 5 (Forward Closure Checking)**.** *Let Lv_i be the candidates generated at level i in Algorithm 4, if FC_i is a proper pattern, then it is safe to terminate Algorithm 4 and directly output FC_i.*

It is notable that, as the level grows in Algorithm 4, the closure FC reduces, thus the terminating power of FC would be stronger. We give hybrid example of the three optimization as follows:

Example 5. *We use Figure 5 (c) to demonstrate the power of candidate pruning. As shown, at the initial stage, $\{3, 6 : 3\}$ is first pruned by Edge Simplification since its timestamps fails to be a candidate sequence. Subsequently, all further candidates containing $\{3, 6\}$ are pruned by Temporal Monotonicity. Then, we check the Forward Closure of remaining candidates (i.e., $\{3, 4\}$ and $\{3, 5\}$) and find $\{3, 4, 5\}$ is a valid candidate. Therefore, $\{3, 4\}$ and $\{3, 5\}$ are pruned, and $\{3, 4, 5\}$ is the output.*

5.3 Correctness of SPARE

We summarize the workflow of SPARE framework in Figure 5 as follows. After the parallel clustering in each snapshot, we build an aggregated graph G_A to capture the clustering relationship. In the map phrase, we partition G_A into stars and emit the star partitions to the reducers. Each reducer is an Apriori Enumerator. When receiving a star Sr_i, the reducer creates initial candidate patterns. Specifically, for each $o \in Sr_i$, a pattern candidate $\{o, i : e(o, i)\}$ is created. Then the Apriori algorithm enumerate the true patterns from the candidate patterns. Meanwhile, the *simplification*, *monotonicity pruning* and *forward closure checking* are applied to boost the enumeration process.

In the following, we show the correctness of the SPARE framework.

Theorem 6. *The SPARE framework guarantees completeness and soundness.*

Proof. If P is a valid pattern in original trajectories, let s be the object with smallest ID in $P.O$. Based on the definition of GCMP, $\forall t \in P.T$, $\forall o \in P.O$, $C_t(s) = C_t(o)$. It follows that all object $o \in P.O$ are in Sr_s. Furthermore, every timestamp in $P.T$ is included in Sr_s. Therefore, P is a valid pattern in Sr_s. This ensures the *completeness*. For any pattern P enumerated by SPARE, by definition of star partition, $\forall o_1, o_2 \in P.O$, $\forall t \in P.T$, $C_t(o_1) = C_t(o_2)$. This ensure the *soundness*. ☐

.

In fact, besides that every valid patterns can be mined in some stars, star partition further ensures that patterns discovered from different star partitions cannot be the same. This can be formulated as:

Lemma 7 (Pattern Uniqueness of Star Partition)**.** *Let Sr_i and Sr_j $(i \neq j)$ be two star partitions. Let P_i (resp. P_j) be the patterns discovered from Sr_i (resp. Sr_j). Then, $\forall p_i \in P_i, \forall p_j \in P_j$, we have $p_i.O \not\equiv p_j.O$.*

Proof. The correctness of Lemma 7 can be directly derived from the above arguments: let o_i be the smallest element in $p_i.O$ and o_j be the smallest element in $p_j.O$. Since p_i and p_j belongs to different stars, then $o_i \neq o_j$, therefore $p_i.O \not\equiv p_j.O$. This proves the lemma. ☐

This lemma verifies the superiority of the SPARE framework over the TRPM framework.

6. EXPERIMENTAL STUDY

6.1 Experimental Setup

We adapt one of the most popular MapReduce platform, Apache Spark, to conduct experiments on mining GCMPs. Our experiments run on a 9-node cluster, with Apache Yarn as the cluster manager. We use 1 node for Yarn resource manager, and use the remaining 8 nodes as executors. Each node in the cluster is uniformly equipped with a 2.2GHz quad-core CPU with 32 GB memory. Inter-node communication is carried by the 1Gbps Ethernet. Some critical configuration of Spark is as follows:

Parameter	Value
Java Version	1.7.0
spark.driver.memory	2GB
spark.executor.cores	2
spark.executor.instances	11
spark.executor.memory	7GB
spark.master	yarn-cluster
spark.serializer	KryoSerializer

We prepare three real datasets for study. The details of the datasets are as follows:

- Geolife [4]: contains 18,670 GPS trajectories for passengers in Beijing over three years. The data are collected per 1 5 seconds. We use linear interpretation for missing data in short-intervals (i.e., 5 seconds), since interpolating big intervals introduces large errors.

- ACTShopping [5]: contains visitors trajectories in ATC shopping center in Osaka from October 24, 2012 to November 29, 2013. There are in total 18670 trajectories, with 41 million data points.

- SingTaxi: contains 15,054 Singapore taxi trajectories in August 2012.

The summary of statistics are presented as in the following table:

6.2 Effects of G on GCMP

We study the effects of the gap parameter G on discovering co-movement patterns. As shown in Figure 3, existing works are not able to handle large trajectories, we sample and cluster 1 million trajectory points from the three real

[4]http://research.microsoft.com/en-us/projects/geolife/
[5]http://www.irc.atr.jp/crest2010_HRI/ATC_dataset/

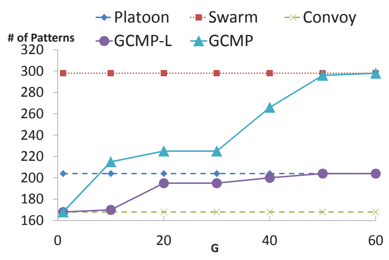

(a) Geolife

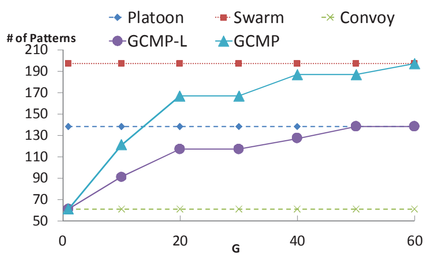

(b) ACTShopping

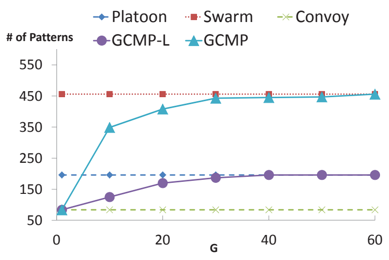

(c) SingTaxi

Figure 8: Effectiveness of GCMP model on sampled datasets.

Table 4: Statistics of data set

	Geolife	ACTShopping	SingTaxi
# objects	18,670	13,183	15,054
# average ts	2,924	3,114	19,667
# longest ts	17,281	24,407	43,717
# data points	54,594,696	41,052,242	296,075,837

Variables	**Meaning**	**Values**
M	min size of object set	20, 40, **60**,80,100
K	min duration	60, 120, **180**, 240, 300
L	min local duration	10, 20, **30**, 40,50
G	max gap	5,10,**15**,20,25
ϵ	DBSCAN parameter	3,6,**9**,12
minPt	DBSCAN parameter	3,6,**9**,12

Table 5: Pattern Parameters and their default values.

data. We use two instances of GCMPs, GCMP-L where the L value is default and GCMP where $L = 1$. We measure the number of patterns discvoered by different methods. The results are presented in Figure 8.

We can see from Figures 8 that the number of patterns discovered by GCMP is a positively related to G. When $G = 1$, the number of patterns returned by GCMP and GCMP-L are identical to *convoy*. As G grows, the number returned by GCMP-L converges to *platoon*. For example, in (a), two patterns converge when G is 40. Similarly in (b) and (c), two patterns converge when G is 50. The reason is that when G is large enough, all consecutive segments in *platoon* satisfy the G-connectivity. Similar trend applies between GCMP and *swarm*. As see from the figures, in (a), two patterns converge at $G = 50$; while in (b) and (c) the two patterns converge at $G = 60$ and $G = 40$ respectively. We further note that, existing patterns has different granularity in temporal domain. As we seen from the three figures, the number of *swarm* is greater than *platoon* and *convoy*. Despite none of the existing patterns are able to fine-grain control the temporal domain of patterns, GCMP can discover the patterns more precisely. These results confirms the usefulness of GCMP in expressing other patterns.

6.3 Performance Comparison

We now study the performance of our GCMP methods. We use TRPM as the baseline algorithm and implement SPM and SPM+.

6.3.1 *Effects of clusters ϵ, minPt*

6.3.2 *Effects of pattern parameters M, L, K, G*

6.4 SPM Analysis

6.4.1 *Load Balance*

6.4.2 *Scalability*

7. CONCLUSION AND FUTURE WORK

8. REFERENCES

[1] Y. Zheng, Y. Liu, J. Yuan, and X. Xie, “Urban computing with taxicabs,” in *Proceedings of the 13th international conference on Ubiquitous computing*, pp. 89–98, ACM, 2011.

[2] Z. Li, B. Ding, J. Han, R. Kays, and P. Nye, “Mining periodic behaviors for moving objects,” in *Proceedings of the 16th ACM SIGKDD international conference on Knowledge discovery and data mining*, pp. 1099–1108, ACM, 2010.

[3] J. Bao, Y. Zheng, D. Wilkie, and M. F. Mokbel, “A survey on recommendations in locationbased social networks. submitted to,” *Geoinformatica*, 2013.

[4] X. Li, *Managing moving objects and their trajectories*. PhD thesis, National University of Singapore, 2013.

[5] J. Gudmundsson and M. van Kreveld, “Computing longest duration flocks in trajectory data,” in *Proceedings of the 14th annual ACM international symposium on Advances in geographic information systems*, pp. 35–42, ACM, 2006.

[6] Y. Wang, E.-P. Lim, and S.-Y. Hwang, “Efficient mining of group patterns from user movement data,” *Data & Knowledge Engineering*, vol. 57, no. 3, pp. 240–282, 2006.

[7] H. Jeung, M. L. Yiu, X. Zhou, C. S. Jensen, and H. T. Shen, “Discovery of convoys in trajectory databases,” *Proceedings of the VLDB Endowment*, vol. 1, no. 1, pp. 1068–1080, 2008.

[8] Z. Li, B. Ding, J. Han, and R. Kays, “Swarm: Mining relaxed temporal moving object clusters,” *Proceedings of the VLDB Endowment*, vol. 3, no. 1-2, pp. 723–734, 2010.

[9] Y. Li, J. Bailey, and L. Kulik, “Efficient mining of platoon patterns in trajectory databases,” *Data & Knowledge Engineering*, 2015.

[10] J. Gudmundsson, M. van Kreveld, and B. Speckmann, “Efficient detection of motion patterns in spatio-temporal data sets,” in *Proceedings of the 12th annual ACM international workshop on Geographic information systems*, pp. 250–257, ACM, 2004.

[11] Y. Zheng, “Trajectory data mining: an overview,” *ACM Transactions on Intelligent Systems and Technology (TIST)*, vol. 6, no. 3, p. 29, 2015.

[12] D. Birant and A. Kut, “St-dbscan: An algorithm for clustering spatial–temporal data,” *Data & Knowledge Engineering*, vol. 60, no. 1, pp. 208–221, 2007.

[13] P. Laube, M. van Kreveld, and S. Imfeld, “Finding remodetecting relative motion patterns in geospatial lifelines,” in *Developments in spatial data handling*, pp. 201–215, Springer, 2005.

[14] D. H. Douglas and T. K. Peucker, “Algorithms for the reduction of the number of points required to represent a digitized line or its caricature,” *Cartographica: The International Journal for Geographic Information and Geovisualization*, vol. 10, no. 2, pp. 112–122, 1973. doi:10.3138/FM57-6770-U75U-7727.

[15] J. Dean and S. Ghemawat, “Mapreduce: simplified data processing on large clusters,” *Communications of the ACM*, vol. 51, no. 1, pp. 107–113, 2008.

[16] Y. Kwon, M. Balazinska, B. Howe, and J. Rolia, “Skewtune: mitigating skew in mapreduce applications,” in *Proceedings of the 2012 ACM SIGMOD International Conference on Management of Data*, pp. 25–36, ACM, 2012.

[17] R. S. Xin, J. Rosen, M. Zaharia, M. J. Franklin, S. Shenker, and I. Stoica, “Shark: Sql and rich analytics at scale,” in *Proceedings of the 2013 ACM SIGMOD International Conference on Management of data*, pp. 13–24, ACM, 2013.

[18] E. Coppa and I. Finocchi, “On data skewness, stragglers, and mapreduce progress indicators,” in *Proceedings of the Sixth ACM Symposium on Cloud Computing*, pp. 139–152, ACM, 2015.

APPENDIX

A. PROOFS OF THEOREMS

A.1 Proof of Theorem 1

A.2 Proof of Theorem 6 and Lemma 7

A.3 Proof of Theorem 5.1

Proof. Let $B*$ be the assignment matrix wrt the optimal numbering. Since we have a star for each object, by the degree-sum formula and pigeon-hole theorem, $\Gamma^* = ||B^*\vec{b}||_\infty \geq d/2$. Next, given a numbering P, let $e_{i,j}$ be an entry in PAP^T. Since edges in graph G are independent, then $e_{i,j}$s are independent. Moreover, let d_i denote the degree of vertex i, then $E[d_i] = E[\Sigma_{1\leq j\leq n} e_{i,j}] = d$. This is because renumbering the vertexes does not affect the average degree. Since $B = \text{triu}(PAP^T)$, entries in B can be written as :

$$b_{i,j} = \begin{cases} e_{i,j}, i > j \\ 0, otherwise \end{cases}$$

There are two observations made. First, since $e_{i,j}$s are independent, $b_{i,j}$s are independent. Second, since $i > j$ and $e_{i,j}$s are independent. $E[b_{i,j}] = E[e_{i,j}]E[i > j] = E[e_{i,j}]/2$.

By definition, $c_i = \Sigma_{1\leq j\leq n} b_{i,j}$, is a sum of n independent 0-1 variables. Taking expectation on both sides, we get: $E[c_i] = E[\Sigma_{1\leq j\leq n} b_{i,j}] = E[\Sigma_{1\leq j\leq n} e_{i,j}]/2 = d/2$. Let $\mu = E[c_i] = d/2$, $t = \sqrt{n \log n}$, by Hoeffding's Inequality, the following holds:

$$\begin{aligned} Pr(c_i \geq \mu + t) &\leq \exp(\frac{-2t^2}{n}) \\ &= \exp(-2\log n) = n^{-2} \end{aligned}$$

The first step is due to the fact that all $b_{i,j}$ are bounded in the range of [0,1]. Next, since the event $(\max_{1\leq j\leq n}(c_j) \geq \mu + t)$ can be viewed as $\cup_{c_i}(c_i \geq \mu + t)$, by Union Bound, we achieve the following:

$$\begin{aligned} Pr(\Gamma \geq \mu + t) &= Pr(\max_{1\leq j\leq n}(c_j) \geq \mu + t) \\ &= Pr(\cup_{c_i}(c_i \geq \mu + t)) \\ &\leq \Sigma_{1\leq i\leq n} Pr(c_i \geq \mu + t) \\ &= n^{-1} = 1/n \end{aligned}$$

Substitute back t and μ, we achieve the following concise form:

$$Pr(\Gamma \geq (d/2 + \sqrt{n \log n})) \leq 1/n$$

This indicates that, the probability of $(\Gamma - d/2)$ being less than or equal to $O(\sqrt{n \log n})$ is $(1 - 1/n)$. With the fact that $\Gamma^* \geq d/2$, we conclude that with probability greater than $(1 - 1/n)$, the difference between Γ and Γ^* is less than $O(\sqrt{n \log n})$. When the aggregated graph is *dense* (i.e., $d \geq \sqrt{12 \log n}$), we may use the Chernoff Bound instead of Hoeffding's Inequality to derive a tighter bound of $O(\sqrt{\log n})$ with the similar reasoning. ☐

A.4 Proof of Theorem 5

Proof. We prove by contradiction. Suppose there exists another pattern P such that $P.O \neq FC_i$, let $X = P.O - FC_i \neq \emptyset$. Consider a subset P_1 of P which contains X with size $i + 1$, (i.e., $P_1 \subseteq P, P_1 \subseteq X, |P_1| = i + 1$). Since P is a proper pattern, then P_1 is also a proper pattern. Therefore $P_1 \in Lv_i$. It follows X is in the forward closure of FC_i, (i.e.,$X \in FC_i$), which contradicts with $X \notin FC_i$. ☐